

# Particle-Hole Transformation in Strongly-Doped Iron-Based Superconductors

J.P. RODRIGUEZ<sup>1</sup>

<sup>1</sup> *Department of Physics and Astronomy, California State University, Los Angeles, California 90032*

PACS 74.70.Xa – Pnictides and chalcogenides  
PACS 74.20.Rp – Pairing symmetries (other than s-wave)  
PACS 74.25.Jb – Electronic structure (photoemission, etc.)

**Abstract** –An exact particle-hole transformation is discovered in a local-moment description of a single layer in an iron-based superconductor. Application of the transformation to a surface layer of heavily electron-doped FeSe predicts a surface-layer high-temperature superconductor at strong hole doping. Comparison with existing low- $T_c$  iron superconductors suggests that the critical temperature at heavy hole doping can be increased by increasing direct ferromagnetic exchange in between nearest neighbor iron atoms.

**Introduction.** – The discovery of iron-based superconductors has identified a new route in the search for high critical temperatures [1]. Iron atoms in these materials lie in weakly coupled stacks of square lattices [2]. Electronic conduction resides within such layers, where charge carriers are primarily electrons/holes from iron  $3d$  levels. The optimum critical temperature in iron-pnictide materials, in particular, coincides with nesting between hole Fermi surfaces pockets at the center of the Brillouin zone and electron Fermi surface pockets at commensurate spin-density wave (cSDW) momenta  $\hbar(\pi/a)\hat{x}$  and  $\hbar(\pi/a)\hat{y}$ . Here,  $\hat{x}$  and  $\hat{y}$  are unit vectors that point along the principal axes of the square lattice of iron atoms, while  $a$  denotes the lattice constant. Strong hole doping can destroy such nesting. In particular, the electron bands at cSDW momenta rise completely above the Fermi level in the series of compounds  $(\text{Ba}_{1-x}\text{K}_x)\text{Fe}_2\text{As}_2$  at  $0.5 < x < 0.7$  [3, 4]. Angle-resolved photoemission spectroscopy (ARPES) on the end-member of the series  $\text{KFe}_2\text{As}_2$ , with  $T_c \cong 4$  K, reveals only hole Fermi surface pockets at zero two-dimensional (2D) momentum [5].

Strong electron doping can also destroy nesting in iron-based superconductors. ARPES on a monolayer of FeSe over a doped  $\text{SrTiO}_3$  (STO) substrate and on intercalated FeSe find only electron Fermi surface pockets at cSDW momenta [6–8]. Hole bands at the center of the Brillouin zone lie buried below the Fermi level. Unlike heavily hole-doped compounds like  $\text{KFe}_2\text{As}_2$ , however, the FeSe surface layer shows high critical temperatures,  $T_c \sim 40 - 100$  K [9, 10]. In addition, ARPES [7, 8] and scanning tunneling microscopy (STM) [11, 12] on such surface layers of FeSe find evidence for an isotropic gap over the electron Fermi surface pockets, with no nodes. Last, a Mott insulator phase is reported nearby at low electron doping in single-layer FeSe/STO and in voltage-gate tuned thin films of FeSe [13, 14]. This indicates that the limit of strong on-site electron repulsion [15, 16] is a valid starting point

filling, bands	$J_1^\parallel < J_1^\perp$	$J_1^\parallel > J_1^\perp$
half filling, none hole dope, hole bands @ $\Gamma$ $e^-$ dope, $e^-$ bands @ M	hidden ferromagnet: $(\pi, 0, 0)$ hidden half metal, FS @ $\Gamma$ nested cSDW metal?	hidden Néel: $(\pi, \pi/a, \pi/a)$ nested cSDW metal? hidden half metal, FS at M

Table 1: Groundstate of two-orbital  $t$ - $J$  model (1). Hund coupling is tuned to the QCP at half filling, which separates a cSDW at strong Hund coupling from hidden magnetic order at weak Hund coupling (ref. [17]). The 3-vector  $(\pi, Q_x, Q_y)$  describes the hidden magnetic order.

to describe superconductivity in heavily electron-doped FeSe.

Below, we identify a particle-hole transformation of a local-moment description for a single layer in an iron-based superconductor [15–17]. The  $t$ - $J$  model that results includes the minimum  $d_{xz}$  and  $d_{yz}$  iron orbitals [18, 19]. Above half filling (electron doping), mean field and exact calculations based on a hidden half metal state that it harbors predict electronic structure that is very similar to that shown by high- $T_c$  surface layers of FeSe [20]. The exact calculations also predict isotropic Cooper pairs at the electron Fermi surface pockets, in addition to remnant isotropic Cooper pairs of opposite sign on buried hole bands. Application of the particle-hole transformation to a surface layer of FeSe predicts a surface-layer iron-based superconductor that is heavily hole-doped, and that exhibits high  $T_c$  [21]. We suggest that heavily hole-doped iron superconductors such as  $\text{KFe}_2\text{As}_2$  show relatively low critical temperatures because of non-ideal Heisenberg exchange coupling constants.

**Local Moment Hamiltonian.** – Our starting point is a two-orbital  $t$ - $J$  model over the square lattice, where on-site-orbital Coulomb repulsion is infinitely strong [18, 19]:

$$\begin{aligned}
H = & \sum_{\langle i, j \rangle} [-(t_1^{\alpha, \beta} c_{i, \alpha, s}^\dagger c_{j, \beta, s} + \text{h.c.}) + J_1^{\alpha, \beta} \mathbf{S}_{i, \alpha} \cdot \mathbf{S}_{j, \beta}] + \\
& \sum_{\langle\langle i, j \rangle\rangle} [-(t_2^{\alpha, \beta} c_{i, \alpha, s}^\dagger c_{j, \beta, s} + \text{h.c.}) + J_2^{\alpha, \beta} \mathbf{S}_{i, \alpha} \cdot \mathbf{S}_{j, \beta}] + \\
& \sum_i (J_0 \mathbf{S}_{i, d-} \cdot \mathbf{S}_{i, d+} + U'_0 \bar{n}_{i, d+} \bar{n}_{i, d-} + \lim_{U_0 \rightarrow \infty} U_0 n_{i, \alpha, \uparrow} n_{i, \alpha, \downarrow}). \quad (1)
\end{aligned}$$

Above,  $\mathbf{S}_{i, \alpha}$  is the spin operator that acts on spin  $s_0 = 1/2$  states of  $d- = d_{(x-iy)z}$  and  $d+ = d_{(x+iy)z}$  orbitals  $\alpha$  in iron atoms at sites  $i$ . Repeated orbital and spin indices in (1) are summed over. Nearest neighbor and next-nearest neighbor Heisenberg exchange across the links  $\langle i, j \rangle$  and  $\langle\langle i, j \rangle\rangle$  is controlled by the coupling constants  $J_1^{\alpha, \beta}$  and  $J_2^{\alpha, \beta}$ , respectively. Hopping of an electron in orbital  $\alpha$  to an unoccupied neighboring orbital  $\beta$  is controlled by the matrix elements  $t_1^{\alpha, \beta}$  and  $t_2^{\alpha, \beta}$ . Finally,  $J_0$  is a ferromagnetic exchange coupling constant that imposes Hund's Rule. The last term in (1) suppresses double occupancy at a site-orbital, where  $n_{i, \alpha, s} = c_{i, \alpha, s}^\dagger c_{i, \alpha, s}$  is the occupation operator for a spin- $s$  electron in orbital  $\alpha$  at site  $i$ . The next-to-last term in (1) measures the energy cost,  $U'_0 > 0$ , of a pair of holes at an iron site, on the other hand, where  $\bar{n}_{i, \alpha} = 1 - \sum_s n_{i, \alpha, s}$  counts holes at site-orbitals below half filling. Observe that  $\bar{n}_{i, \alpha}$  can be replaced by  $-\bar{n}_{i, \alpha}$ , which counts singlet pairs at site-orbitals above half filling. Last, notice that the operation  $d\pm \rightarrow e^{\pm i\theta} d\pm$  is equivalent to a rotation of the orbitals by an angle  $\theta$  about the  $z$  axis. Spin and occupation operators remain invariant under it. Magnetism described by the two-orbital  $t$ - $J$  model (1) is hence isotropic, which suppresses orbital order and nematicity [22].

Because the spin-1/2 moments live on isotropic  $d\pm$  orbitals, two isotropic nearest neighbor and next-nearest neighbor Heisenberg exchange coupling constants exist:

$$J_n^\parallel = J_n^{d\pm, d\pm} \quad \text{and} \quad J_n^\perp = J_n^{d\pm, d\mp} \quad (n = 1, 2). \quad (2)$$

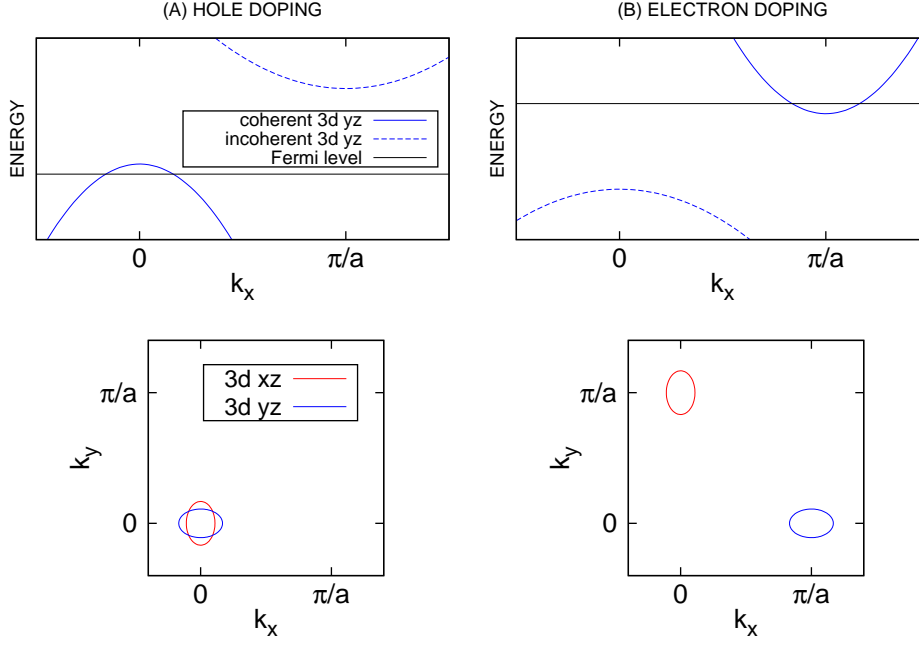


Fig. 1: Electronic structure of half metal states characterized by hidden magnetic order depicted by insets to Fig. 2. Dispersions in energy are fixed at wavenumber  $k_y = 0$ .

The isotropy of the  $d_{\pm}$  orbitals also implies intra-orbital hopping matrix elements that are isotropic and real:  $t_n^{\parallel} = t_n^{d_{\pm}, d_{\pm}}$  for  $n = 1, 2$ . Finally, the reflection properties of the  $d_{xz}$  and  $d_{yz}$  orbitals also imply real inter-orbital hopping matrix elements between nearest neighbors with  $d$ -wave symmetry [19]:  $t_1^{\perp}(\hat{x}) = -t_1^{\perp}(\hat{y})$ , where  $t_1^{\perp} = t_1^{d_{\pm}, d_{\mp}}$ . Inter-orbital next-nearest neighbor hopping matrix elements  $t_2^{d_{\pm}, d_{\mp}}$  also show  $d$ -wave symmetry, but they are pure imaginary. They consequently result in hybridization of the  $d_{xz}$  and  $d_{yz}$  orbital bands. Table 1 summarizes the expected phase diagram of the two-orbital  $t$ - $J$  model (1) near a quantum critical point into hidden magnetic order [17].

**Particle-Hole Transformation.** — We first define the particle-hole transformation that is relevant to iron-based high-temperature superconductors in momentum space for electrons in either the  $d_{xz}$  or  $d_{yz}$  orbitals. The corresponding electron destruction operator reads

$$c_s(k_0, \mathbf{k}) = \mathcal{N}^{-1/2} \sum_{\alpha=0}^1 \sum_i e^{-i(k_0 \alpha + \mathbf{k} \cdot \mathbf{r}_i)} c_{i, \alpha, s}, \quad (3)$$

where  $\mathcal{N} = 2N_{\text{Fe}}$  denotes the number of sites-orbitals on the square lattice of iron atoms, and where the indices 0 and 1 denote the  $d_-$  and  $d_+$  orbitals  $\alpha$ . The quantum numbers  $k_0 = 0$  and  $\pi$  therefore represent the  $d_{xz}$  and the  $(-i)d_{yz}$  orbitals. We then define the particle-hole transformation by the replacements

$$c_s(k_0, \mathbf{k}) \rightarrow c_s(k_0, \mathbf{k} + \mathbf{Q}_{k_0})^{\dagger} \quad \text{and} \quad c_s(k_0, \mathbf{k})^{\dagger} \rightarrow c_s(k_0, \mathbf{k} + \mathbf{Q}_{k_0}), \quad (4)$$

where  $\mathbf{Q}_0 = (\pi/a)\hat{y}$  and  $\mathbf{Q}_{\pi} = (\pi/a)\hat{x}$ . Figure 1 displays the action of the above transformation on electronic structure. What then is the form of the above particle-hole transformation in real space for electrons in  $d_{\pm}$  orbitals? Comparison of (3) and (4) yields the equivalent particle-hole transformation in real space:

$$c_{i, \alpha, s} \rightarrow (-1)^{y_i/a} c_{i, p_i(\alpha), s}^{\dagger} \quad \text{and} \quad c_{i, \alpha, s}^{\dagger} \rightarrow (-1)^{y_i/a} c_{i, p_i(\alpha), s} \quad (5)$$

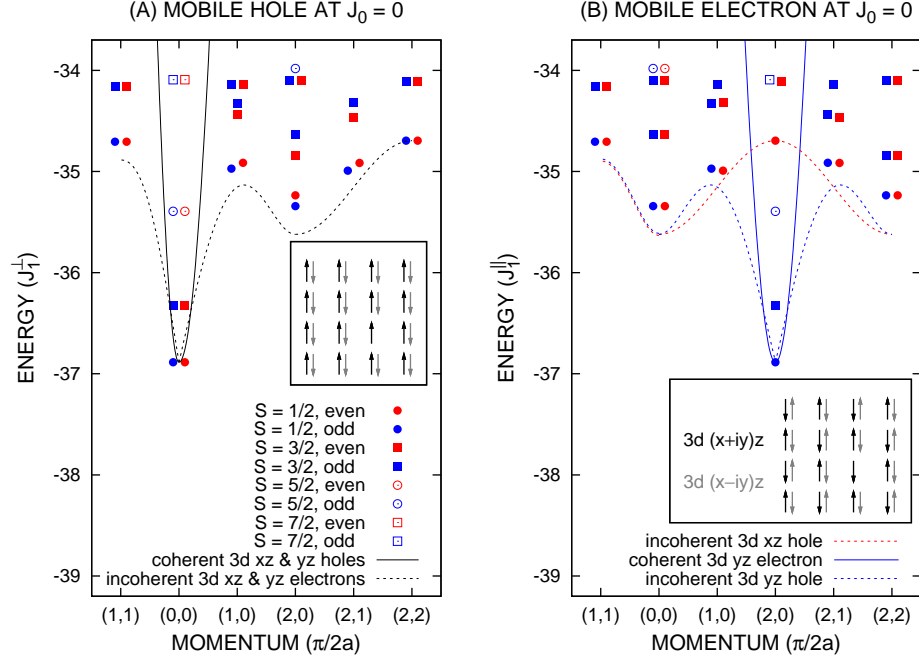


Fig. 2: Exact spectra for  $t$ - $J$  model, Eq. (1), over a periodic  $4 \times 4$  lattice, with parameters (a)  $J_1^\parallel = 0$ ,  $J_1^\perp > 0$ ,  $J_2^\parallel = 0.3 J_1^\perp = J_2^\perp$ ,  $t_1^\parallel = -3 J_1^\perp$ ,  $t_1^\perp(\hat{x}) = -2 J_1^\perp$ ,  $t_1^\perp(\hat{y}) = +2 J_1^\perp$ ,  $t_2^\parallel = -J_1^\perp$ , and  $t_2^{d\pm, d\mp} = 0$  in the mobile-hole case. Model parameters transform to (b)  $J_1^\parallel > 0$ ,  $J_1^\perp = 0$ ,  $J_2^\parallel = 0.3 J_1^\parallel = J_2^\perp$ ,  $t_1^\parallel = 2 J_1^\parallel$ ,  $t_1^\perp(\hat{x}) = +3 J_1^\parallel$ ,  $t_1^\perp(\hat{y}) = -3 J_1^\parallel$ ,  $t_2^\parallel = -J_1^\parallel$ , and  $t_2^{d\pm, d\mp} = 0$  in the mobile-electron case.

where  $p_i(d\pm) = d\pm$  for iron sites  $i$  on the  $A$  sublattice of the checkerboard, and where  $p_i(d\pm) = d\mp$  for iron sites  $i$  on the  $B$  sublattice of the checkerboard.

Making the replacements (5) in the two-orbital  $t$ - $J$  model Hamiltonian (1) maintains its form. Nearest neighbor model parameters, however, transform to

$$\begin{aligned} \bar{J}_1^\parallel &= J_1^\perp & \text{and} & & \bar{J}_1^\perp &= J_1^\parallel, \\ \bar{t}_1^\parallel &= -t_1^\perp(\hat{x}) & \text{and} & & \bar{t}_1^\perp(\hat{x}) &= -t_1^\parallel, \end{aligned} \quad (6)$$

with  $\bar{t}_1^\perp(\hat{y}) = -\bar{t}_1^\perp(\hat{x})$ . Next-nearest neighbor model parameters  $t_2^\parallel$ ,  $J_2^\parallel$  and  $J_2^\perp$  remain unchanged, while corresponding inter-orbital hopping matrix elements, which are pure imaginary with  $d$ -wave symmetry [19], transform to

$$\bar{t}_2^{d\pm, d\mp}|_A = +t_2^{d\pm, d\mp}|_A \quad \text{and} \quad \bar{t}_2^{d\pm, d\mp}|_B = -t_2^{d\pm, d\mp}|_B. \quad (7)$$

Last, on-site parameters  $J_0$ ,  $U_0$  and  $U'_0$  for ferromagnetic Hund coupling and for Coulomb repulsion also remain unchanged. Here, the occupation operators  $n_{i,\alpha,s}$  in the divergent Hubbard term must be replaced by  $1 - n_{i,\alpha,s}$ .

**Emergent Electron/Hole Bands.** — We shall now compare spectra for one mobile hole and for one mobile electron, with  $t$ - $J$  model parameters that are related to each other by the previous particle-hole transformation. In the hole-doped case, the Heisenberg exchange coupling constants are set to  $J_1^\parallel = 0$ ,  $J_1^\perp > 0$ , and  $J_2^\parallel = 0.3 J_1^\perp = J_2^\perp$ , while the hopping matrix elements are set to  $t_1^\parallel = -3 J_1^\perp$ ,  $t_1^\perp(\hat{x}) = -2 J_1^\perp$ ,  $t_1^\perp(\hat{y}) = +2 J_1^\perp$ ,  $t_2^\parallel = -J_1^\perp$  and  $t_2^{d\pm, d\mp} = 0$ . The latter turns off hybridization between the  $d_{xz}$  and  $d_{yz}$  orbital bands. In the electron-doped case, nearest neighbor  $t$ - $J$  model parameters are set by (6), while on-site

and next-nearest neighbor model parameters are unchanged. Figure 2 shows exact spectra for one mobile hole and for one mobile electron roaming over a periodic  $4 \times 4$  lattice of iron atoms, in the absence of Hund's Rule,  $J_0 = 0$ . Details of the numerical calculation are given in the Supplemental Material and in ref. [19]. Notice that all of the states obey the particle-hole transformation (4). Figure 3 shows the one-hole and one-electron spectra at Hund coupling  $-J_0 = 2.04 J_1^{(\perp)\parallel}$ . All states again satisfy the particle-hole relationship (4).

The dispersion of the lowest-energy spin-1/2 mobile-hole states shown by Fig. 2a can be understood at ideal hopping, achieved by suppressing inter-orbital hopping:  $t_1^\perp \rightarrow 0$ . A half metal characterized by hidden magnetic order depicted by the inset to Fig. 2a is predicted in the absence of Hund's Rule at large electron spin  $s_0$  [18,19]. Electrons are spin polarized per  $d\pm$  orbital, where they follow a hole-type energy dispersion relation

$$\varepsilon_e^{(0)}(\mathbf{k}) = -2t_1^\parallel(\cos k_x a + \cos k_y a) - 2t_2^\parallel(\cos k_+ a + \cos k_- a), \quad (8)$$

with  $k_\pm = k_x \pm k_y$ . Two degenerate hole Fermi surface pockets at zero 2D moment are predicted for small concentrations of mobile holes per orbital,  $x$ , each with a Fermi wavenumber  $k_F a = (4\pi x)^{1/2}$ . The top of the hole-type band (8) lies  $\epsilon_F = |t_1^\parallel + 2t_2^\parallel|(k_F a)^2$  above the Fermi level. The one-electron propagator can be calculated within a Schwinger-boson-slave-fermion mean-field approximation of the two-orbital  $t$ - $J$  model (1) for the above hidden half metal [18,19]. In the limit near half filling, at  $|t| \gg J$ , it reveals composite electron-spin-wave states at an energy  $\epsilon_F + \hbar\omega_{\text{sw}}(\mathbf{k})$  above the Fermi level, where  $\omega_{\text{sw}}(\mathbf{k})$  is the spin-wave dispersion at large electron spin  $s_0$  [17]. (See Supplemental Material and ref. [21].) The predicted dispersion relation is traced by the dashed line in Fig. 2a. It compares well with the exact dispersion of the lowest-energy spin-1/2 excitations at non-ideal hopping matrix elements, in the absence of Hund's Rule, and it notably shows electron-type dispersion in the vicinity of cSDW wavenumbers  $(\pi/a)\hat{\mathbf{x}}$  and  $(\pi/a)\hat{\mathbf{y}}$ . We therefore interpret the dispersion of those spin-1/2 groundstates, which respectively have even and odd parity under orbital swap  $P_{d,\bar{d}}$ , as emergent  $d_{xz}$  and  $d_{yz}$  electron bands. Figure 3a indicates that nesting of the coherent hole bands (8) with the emergent electron bands begins at a critical value of Hund coupling.

Application of the particle-hole transformation (5) yields a new half metal state depicted by the inset to Fig. 2b, where the missing spin-1/2 moment in the third row represents a spin singlet. It is governed by the two-orbital  $t$ - $J$  model (1) at electron doping above half-filling, with a new set of parameters (6)  $J_1^\parallel > 0$ ,  $J_1^\perp = 0$ ,  $t_1^\parallel = +2J_1^\parallel$ ,  $t_1^\perp(\hat{\mathbf{x}}) = +3J_1^\parallel$ ,  $t_1^\perp(\hat{\mathbf{y}}) = -3J_1^\parallel$ ,  $t_2^\parallel = -J_1^\parallel$ , and  $t_2^{d\pm, d\mp} = 0$ . As  $t_1^\parallel \rightarrow 0$ , Schwinger-boson-slave-fermion mean field theory for the half metal state predicts emergent *hole* excitations that disperse according to the dashed lines in Fig. 2b. (See Supplemental Material and ref. [20].) Again, the mean-field results compare well with the exact ones, while Fig. 3b indicates that nesting of the electron bands with the emergent hole bands begins at the prior critical strength in Hund coupling.

**Cooper Pairs with Emergent Sign Changes.** – Consider now two electrons above half filling that roam over a  $4 \times 4$  periodic lattice of iron atoms governed by the two-orbital  $t$ - $J$  model (1) [20]. Heisenberg exchange parameters are set to those listed in the caption to Fig. 2b, but new hopping matrix elements are chosen that leave the electron masses  $m_x$  and  $m_y$  per orbital unchanged at cSDW momenta:  $t_1^\parallel = 2J_1^\parallel$ ,  $t_1^\perp(\hat{\mathbf{x}}) = +5J_1^\parallel$ ,  $t_1^\perp(\hat{\mathbf{y}}) = -5J_1^\parallel$ , and  $t_2^{\alpha,\beta} = 0$ . Such model parameters produce electron-type Fermi surface pockets centered at cSDW momenta in the hidden half metal state within the mean field approximation. Details of the exact calculation are given in the Supplemental Material and in ref. [21]. In the case of one mobile electron, and under the new set of hopping parameters, the low-energy spectrum at the QCP resembles that depicted by Fig. 3b under the previous set of hopping matrix elements, but with emergent hole bands at zero 2D momentum that show small mass anisotropy [20]. In the case of two mobile electrons, the Hund coupling,  $-J_0$ , is tuned to a putative QCP defined by degeneracy of the spin resonance at cSDW momenta with

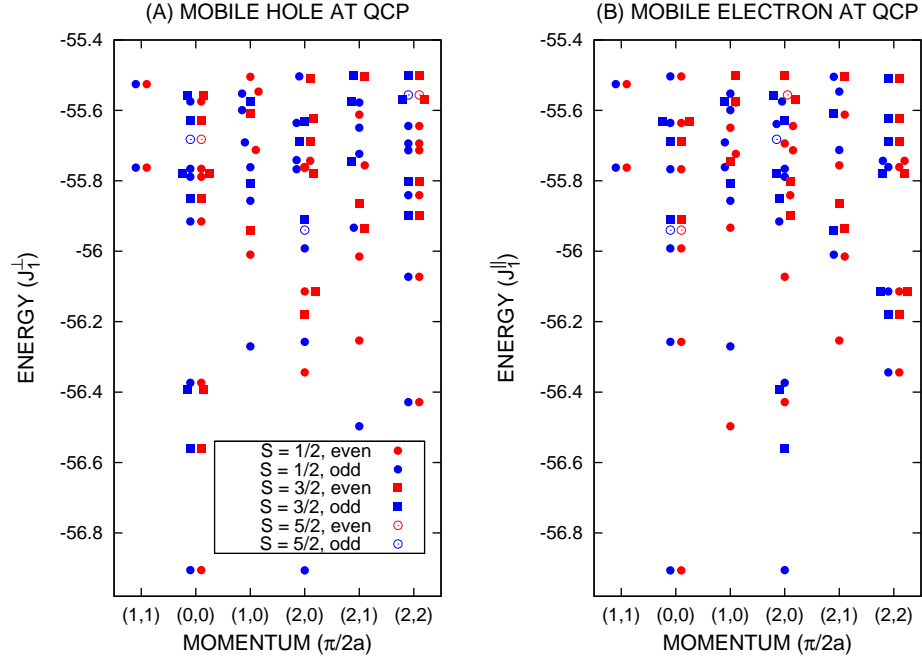


Fig. 3: Exact spectra of two-orbital  $t$ - $J$  model at Hund coupling  $-J_0 = 2.04 J_1^{(\perp)\parallel}$ . The remaining model parameters are given in the caption to Fig. 2.

the lowest-energy spin-1 state at momentum  $(\pi/a)(\hat{x} + \hat{y})$ , which is associated with hidden magnetic order. This definition is suggested by a semi-classical analysis of the corresponding Heisenberg model at half filling, which finds a QCP in such case that separates hidden magnetic order at weak Hund coupling, as depicted by the inset to Fig. 2b, from a cSDW at strong Hund coupling [17]. At zero net 2D momentum, a bound electron-pair groundstate exists below a continuum of states. It shows  $S$ -wave symmetry according to the reflection parities listed in Table 2. An excited pair state with  $D_{x^2-y^2}$  symmetry exists below the continuum as well.

The order parameter for superconductivity is the defined as

$$iF(k_0, \mathbf{k}) = \langle \Psi_{\text{Mott}} | \tilde{c}_{\uparrow}(k_0, \mathbf{k}) \tilde{c}_{\downarrow}(k_0, -\mathbf{k}) | \Psi_{\text{Cooper}} \rangle \quad (9)$$

times  $\sqrt{2}$ , where  $|\Psi_{\text{Cooper}}\rangle$  is the groundstate of the electron pair, and where  $\langle \Psi_{\text{Mott}} |$  is the groundstate of the Mott insulator at half filling. Above, the tilde notation signals the limit  $U_0 \rightarrow \infty$ . Figure 4b depicts (9) using exact groundstates  $\langle \Psi_{\text{Mott}} |$  and  $|\Psi_{\text{Cooper}}\rangle$  on a  $4 \times 4$  periodic lattice of iron atoms at the putative QCP. In particular, the Hund coupling is tuned

Table 2: Reflection parities, orbital-swap parity, and spin of low-energy pair states with zero net momentum in order of increasing energy. The operator  $R_{x'z}$ , for example, denotes a reflection about the  $x'$ - $z$  plane, where  $x'$  is a diagonal axis. The hidden spinwave is exceptional in the case of electron doping, where it carries net momentum  $(\pi/a)(\hat{x} + \hat{y})$ .

no.	Pair State	$R_{xz}, R_{yz}$	$R_{x'z}, R_{y'z}$	$P_{d,\bar{d}}$	spin
0	$S$	+	+	+	0
1	$D_{x^2-y^2}$	+	-	+	0
2	hidden spinwave	-	-	-	1

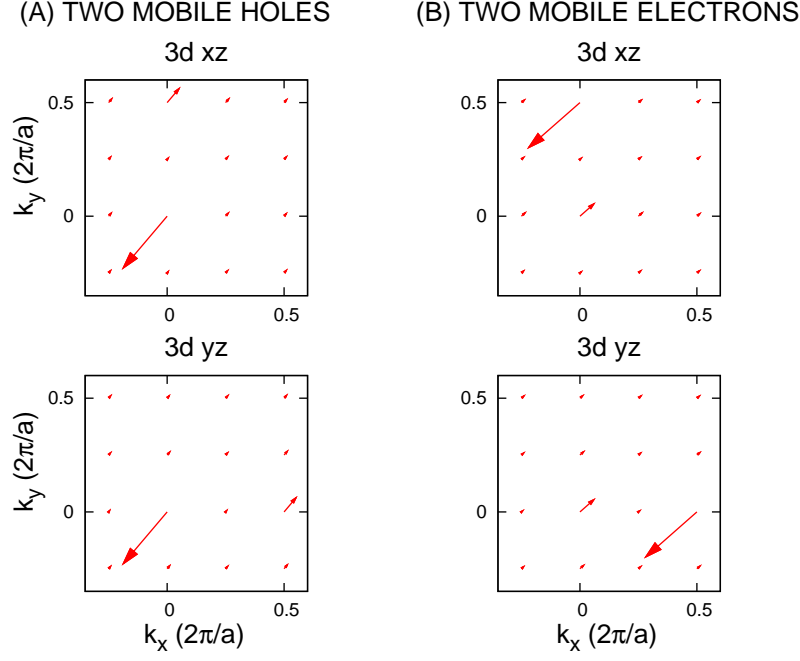


Fig. 4: Complex order parameter for superconductivity, Eq. 9, with Heisenberg exchange coupling constants set in the caption to Fig. 2, and with hopping matrix elements (a)  $t_1^{\parallel} = -5 J_1^{\perp}$ ,  $t_1^{\perp}(\hat{x}) = -2 J_1^{\perp}$ ,  $t_1^{\perp}(\hat{y}) = +2 J_1^{\perp}$ , and  $t_2^{\alpha,\beta} = 0$  for two mobile holes. Nearest neighbor hopping matrix elements transform to (b)  $t_1^{\parallel} = 2 J_1^{\parallel}$ ,  $t_1^{\perp}(\hat{x}) = +5 J_1^{\parallel}$  and  $t_1^{\perp}(\hat{y}) = -5 J_1^{\parallel}$  for two mobile electrons. Also, inter-orbital on-site repulsion is set to  $U'_0 = \frac{1}{4}J_0 + 1000 J_1^{(\perp)\parallel}$ , while the Hund coupling constant is set to  $-J_0 = 2.25 J_1^{(\perp)\parallel}$ . Heisenberg-exchange pairs in the Hamiltonian (1) are replaced with  $1/2$  the corresponding spin-exchange operators to reduce finite-size effects.

so that the groundstate spin-1 states at cSDW momenta, which have even parity under orbital swap,  $P_{d,\vec{a}}$ , become degenerate with the groundstate spin-1 state at wavenumber  $(\pi/a)(\hat{x} + \hat{y})$ , which has odd parity under orbital swap. The coupling constants, respectively, are  $-J_0 = 1.35 J_1^{\parallel}$  and  $-J_0 = 2.25 J_1^{\parallel}$  at half filling and for two mobile electrons. Notice that the order parameter displayed by Fig. 4b is isotropic, but that it alternates in sign between the emergent hole bands at zero 2D momentum and the electron bands at cSDW momenta [20].

Figure 4a shows the particle-hole conjugate of the order parameter (9) for superconductivity in the two-orbital  $t$ - $J$  model with two-mobile holes that roam over a  $4 \times 4$  periodic lattice, under the transformation (6)-(7) in parameter space [21]. Notice that it is related to Fig. 4b by the particle-hole transformation (4). In conclusion, both the electron pair and the conjugate hole pair display an  $S^{+-}$  order parameter for superconductivity, with remnant pairing on the emergent band of opposite sign. This result is similar to a recent proposal for  $S^{+-}$  pairing in heavily hole-doped iron superconductors that is based on a phenomenological attractive pairing interaction [23].

**Discussion and Conclusions.** – The particle-hole transformation (4)/(5) can be applied to strongly electron-doped iron-based superconductors ultimately to predict new iron-based superconductors that are strongly doped by holes. Heavily electron-doped surface layers of FeSe show record critical temperatures as high as  $T_c \cong 100$  K [10]. ARPES reveals two electron pockets at the corner of the two-iron Brillouin zone that cross and do not show level repulsion [7]. The author has recently proposed that the Cooper pairs in these systems



are isotropic, but that they change sign according to Fig. 4b [20]. He describes the electronic structure at the surface layer of FeSe with the two-orbital  $t$ - $J$  model (1) at sub-critical Hund coupling, with hopping matrix elements and Heisenberg exchange coupling constants that favor the half metal state shown in the inset to Fig. 2b. In particular, Schwinger-boson-slave-fermion mean field theory and the exact results displayed by Fig. 3b predict electron Fermi surface pockets centered at the two distinct cSDW momenta. This suggests that the Fermi surface pockets are robust in the presence of hybridization between the  $d_{xz}$  and  $d_{yz}$  orbitals through the addition of inter-orbital hopping to next-nearest neighbors over equivalent iron atoms:  $t_2^{d\pm, d\mp}|_A = t_2^{d\pm, d\mp}|_B$ . The latter are pure imaginary and show  $d$ -wave symmetry [19].

Application of the particle-hole transformation (5) to the two-orbital  $t$ - $J$  model for a surface layer of FeSe implies a heavily hole-doped surface layer that shows hole-type Fermi surface pockets at the center of the Brillouin zone (Fig. 1a) and high- $T_c$  superconductivity. By (7), the difference between the  $A$  and  $B$  iron sites is maximal per next-nearest neighbor inter-orbital hopping parameters, which are pure imaginary:  $\bar{t}_2^{d\pm, d\mp}|_B = -\bar{t}_2^{d\pm, d\mp}|_A$ . Iron-pnictide and iron-chalcogenide layers satisfy the ( $d$ -wave) identities  $t_2^{d\pm, d\mp}(\hat{x}')|_A = -t_2^{d\pm, d\mp}(\hat{y}')|_B$  and  $t_2^{d\pm, d\mp}(\hat{y}')|_A = -t_2^{d\pm, d\mp}(\hat{x}')|_B$ , however, which remain true in the presence of a substrate. Here,  $\hat{x}'$  and  $\hat{y}'$  denote the iron-to-pnictide/chalcogenide directions. The particle-hole transformation,  $\bar{t}_2^{d\pm, d\mp}$ , of the original hopping matrix elements does not satisfy these identities, and it is therefore not valid.

We can, however, consider the action of the particle-hole transformation in the absence of hybridization:  $t_2^{d\pm, d\mp} = 0$ . By table 1 and by (6), Heisenberg exchange coupling constants satisfy  $\bar{J}_1^{\parallel} < \bar{J}_1^{\perp}$  after the electron-hole transformation (5). Non-ideal Heisenberg exchange coupling constants  $\bar{J}_1^{\parallel} > \bar{J}_1^{\perp}$  at hole doping may result in a smaller critical temperature, which could account for the relatively low  $T_c$  of the heavily hole-doped compound  $\text{KFe}_2\text{As}_2$ . Compression of iron atoms on a surface layer can result in direct ferromagnetic exchange, which in turn can help achieve the ideal inequality  $\bar{J}_1^{\parallel} < \bar{J}_1^{\perp}$  at hole doping [19]. The hole-doped series  $\text{Ba}_{1-x}\text{K}_x\text{Fe}_2\text{As}_2$  shows a Lifshitz transition at hole doping beyond the optimum critical temperature, where the electron bands at cSDW momenta rise entirely above the Fermi level [4] following Fig. 1a [21]. The previous observation suggests that the application of bi-axial pressure on  $\text{Ba}_{1-x}\text{K}_x\text{Fe}_2\text{As}_2$  will increase its critical temperature in the vicinity of the Lifshitz transition. (Cf. refs. [24] and [25].)

\* \* \*

The author thanks Miguel Araujo for correspondence. He also thanks Brent Andersen, Richard Roberts and Timothy Sell for technical help with the use of the virtual shared-memory cluster (Lancer) at the AFRL DoD Supercomputing Resource Center. This work was supported in part by the US Air Force Office of Scientific Research under grant no. FA9550-13-1-0118 and by the National Science Foundation under PREM grant no. DMR-1523588.

## REFERENCES

- [1] KAMIHARA Y., WATANABE T., HIRANO M. and HOSONO H., *J. Am. Chem. Soc.*, **130** (2008) 3296.
- [2] PAGLIONE J. and GREENE R.L., *Nat. Phys.*, **6** (2010) 645.
- [3] SATO T., NAKAYAMA K., SEKIBA Y., RICHARD P., XU Y.-M., SOUMA S., TAKAHASHI T., CHEN G.F., LUO J.L., WANG N.L. and DING H., *Phys. Rev. Lett.*, **103** (2009) 047002
- [4] Malaeb W., Shimojima T., Ishida Y., Okazaki K., Ota Y., Ohgushi K., Kihou K., Saito T., Lee C.H., Ishida S., Nakajima M., Uchida S., Fukazawa H., Kohori Y., Iyo A., Eisaki H., Chen C.-T., Watanabe Ikeda S., H., and Shin S., *Phys. Rev. B*, **86** (2012) 165117
- [5] OKAZAKI K., OTA Y., KOTANI Y., MALAEB W., ISHIDA Y., SHIMOJIMA T., KISS T., WATANABE S., CHEN C.-T., KIHOU K., LEE C.H., IYO A., EISAKI H., SAITO T., H. FUKAZAWA, Y.



- KOHORI, K. HASHIMOTO, T. SHIBAUCHI, Y. MATSUDA, H. IKEDA, MIYAHARA H., ARITA R., CHAINANI A. and SHIN S., *Science*, **337** (2012) 1314
- [6] LIU D., ZHANG W., MOU D., HE J., OU Y.-B., WANG Q.-Y., LI Z., WANG L., ZHAO L., HE S., PENG Y., LIU X., CHAOYU C., YU L., LIU G., DONG X., ZHANG J., CHEN C., XU Z., HU J., CHEN X., MA Z., XUE Q. and XHOU X.J., *Nat. Comm.*, **3** (2012) 931
- [7] PENG R., SHEN X.P., XIE X., XU H.C., TAN S.Y., XIA M., ZHANG T., CAO H.Y., GONG X.G., HU J.P., XIE B.P. and FENG D.L., *Phys. Rev. Lett.*, **112** (2014) 107001
- [8] Zhao L., Liang A., Yuan D., Hu Y., Liu D., Huang J., He S., Shen B., Xu Y., Liu X., Yu L., Liu G., Zhou H., Huang Y., Dong X., Zhou F., Zhao Z., Chen C., Xu Z. and Zhou X. *J. Nat. Comm.*, **7** (2016) 10608
- [9] ZHANG W.-H., SUN Y., ZHANG J.-S., LI F.-S., GUO M.-H., ZHAO Y.-F., ZHANG H.-M., PENG J.-P., XING Y., WANG H.-C., FUJITA T., HIRATA A., LI Z., DING H., TANG C.-J., WANG M., WANG Q.-Y., HE K., JI S.-H., CHEN X., WANG J.-F., XIA Z.-C., LI L., WANG Y.-Y., WANG J., WANG L.-L., CHEN M.-W., XUE Q.-K. and MA X.-C., *Chin. Phys. Lett.*, **31** (2014) 017401
- [10] GE J.-F., LIU Z.-L., LIU C., GAO C.-L., QIAN D., XUE Q.-K., LIU Y. and JIA J.-F., *Nat. Mat.*, **14** (2015) 285.
- [11] FAN Q., ZHANG W.H., LIU X., YAN Y.J., REN M.Q., PENG R., XU H.C., XIE B.P., HU J.P., ZHANG T., and FENG D.L., *Nat. Phys.*, **11** (2015) 946
- [12] YAN Y.J. ZHANG W.H., REN M.Q., LIU X., LU X.F., WANG N.Z., NIU X.H., FAN Q., MIAO J., TAO R., XIE B.P., CHEN X.H., ZHANG T. and FENG D.L., *Phys. Rev. B*, **94** (2016) 134502
- [13] HE J., LIU X., ZHANG W., ZHAO L., LIU D., HE S., MOU D., LI F., TANG C., LI Z., WANG L., PENG Y., LIU Y., CHEN C., YU L., LIU G., DONG X., ZHANG J., CHEN C., XU Z., CHEN X., MA X., XUE Q. and ZHOU X.J., *Proc. Nat. Acad. Sci.*, **111** (2014) 18501.
- [14] HANZAWA K., SATO H., KAMIYA T. and HOSONO H., *Proc. Nat. Acad. Sci.*, **113** (2016) 3986
- [15] SI Q. and ABRAHAMS E., *Phys. Rev. Lett.*, **101** (2008) 076401
- [16] RODRIGUEZ J.P. and REZAYI E.H., *Phys. Rev. Lett.*, **103** (2009) 097204
- [17] RODRIGUEZ J.P., *Phys. Rev. B*, **82** (2010) 014505
- [18] RODRIGUEZ J.P., ARAUJO M.A.N. and SACRAMENTO P.D., *Phys. Rev. B*, **84** (2011) 224504
- [19] RODRIGUEZ J.P., ARAUJO M.A.N. and SACRAMENTO P.D., *Eur. Phys. J. B*, **87** (2014) 163
- [20] RODRIGUEZ J.P., arXiv:1601.01860 .
- [21] RODRIGUEZ J.P., *J. Phys.: Condens. Matter*, **28** (2016) 375701
- [22] The two-orbital  $t$ - $J$  model for iron superconductors, Eq. (1), predicts a transition to a Mott insulator state at half filling that can be pre-empted by a transition to nematic order instead. See supplemental material in ref. [21].
- [23] BANG Y., *New J. Phys.*, **16** (2014) 023029
- [24] TAFTI F.F., JUNEAU-FECTEAU A., DELAGE M.-E., RENE DE COTRET S., REID J.-P., WANG A.F., LUO X.-G., CHEN X.H., DOIRON-LEYRAUD N., and TAILLEFER L., *Nat. Phys.*, **9** (2013) 349
- [25] NAKAJIMA Y., WANG R., METZ T., WANG X., WANG L., CYNN H., WEIR S.T., JEFFRIES J.R., and PAGLIONE J., *Phys. Rev. B*, **91** (2015) 060508(R)